# Optimized reforming of biomass derived gas based on thermodynamic and kinetics analysis with activated carbon fibers supported Ni-$Al_2O_3$

**Lei Yu [1], Min Song [1,*], Paul T. Williams [2], Yuexing Wei [1]**

1 Ministry of Education of Key Laboratory of Energy Thermal Conversion and Control, School of Energy and Environment, Southeast University, Nanjing, 210096, China

2 School of Chemical & Process Engineering, University of Leeds, Leeds, LS2 9JT, UK

*Correspondence author: minsong@seu.edu.cn;

**Supplementary material**

TableS1 Volume fraction of various components of different biomass derived gas ($N_2$ free)

| Biomass | Catalysts | $H_2$ | CO | $CH_4$ | $CO_2$ | $C_2$-$C_4$ | Reference |
|---|---|---|---|---|---|---|---|
| Wood Sawdust | 9Ni1FeAl | 36.5 | 41.6 | 6.2 | 14.5 | 1.2 | [S1] |
| | Sand | 17.4 | 45.5 | 14.8 | 14.5 | 7.8 | [S1] |
| Corn Stover | - | 16.20 | 20.88 | 12.19 | 48.85 | 5.72 | [S2] |
| Wood Chips | - | 29.59 | 32.87 | 4.93 | 32.58 | - | [S3] |
| Sawdust | Fe/CaO | 21.5 | 33.5 | 13.0 | 26.5 | 5.5 | [S4] |

Reference:

[S1] Dong L., Wu C., Ling H., Shi J., Williams, P. T., Huang, J. (2016). Development of Fe-promoted Ni-Al catalysts for hydrogen production from gasification of wood sawdust. Energy & Fuels, 31(3), 2118-2127.

[S2] Zhang Y., Ke C., Gao Y., Liu S., Pan Y., Zhou N., Wang Y., Fan L., Peng P., Li B., Ruan R. (2019). Syngas production from microwave-assisted air gasification of biomass: Part 2 model validation. Renewable energy, 140, 625-632.

[S3] Yao Z., You S., Ge T., Wang, C. H. (2018). Biomass gasification for syngas and biochar co-production: Energy application and economic evaluation. Applied Energy, 209, 43-55.

[S4] Yang S., Zhang X., Chen L., Sun L., Xie X., Zhao, B. (2017). Production of syngas from pyrolysis of biomass using Fe/CaO catalysts: effect of operating conditions on the process. Journal of Analytical and Applied Pyrolysis, 125, 1-8.

TableS2 Detailed distribution of components for raw gas (Catalyst dosage: 0.5g; Reaction temperature: 800℃; WHSV: 24000 mL•$h^{-1}$•$gcat^{-1}$)

| Components | Flow rate(mL/min) | | | | |
|---|---|---|---|---|---|
| | $CH_4$ | $CO_2$ | CO | $H_2$ | $N_2$ |
| Effect of $CH_4$ | 20 | 50 | 0 | 0 | 130 |
| | 40 | 50 | 0 | 0 | 110 |
| | 60 | 50 | 0 | 0 | 90 |
| | 80 | 50 | 0 | 0 | 70 |
| Effect of $CO_2$ | 50 | 20 | 0 | 0 | 130 |
| | 50 | 40 | 0 | 0 | 110 |
| | 50 | 60 | 0 | 0 | 90 |
| | 50 | 80 | 0 | 0 | 70 |
| Effect of CO | 50 | 50 | 20 | 0 | 80 |
| | 50 | 50 | 40 | 0 | 60 |
| | 50 | 50 | 60 | 0 | 40 |
| | 50 | 50 | 80 | 0 | 20 |
| Effect of $H_2$ | 50 | 50 | 0 | 20 | 80 |
| | 50 | 50 | 0 | 40 | 60 |
| | 50 | 50 | 0 | 60 | 40 |
| | 50 | 50 | 0 | 80 | 20 |

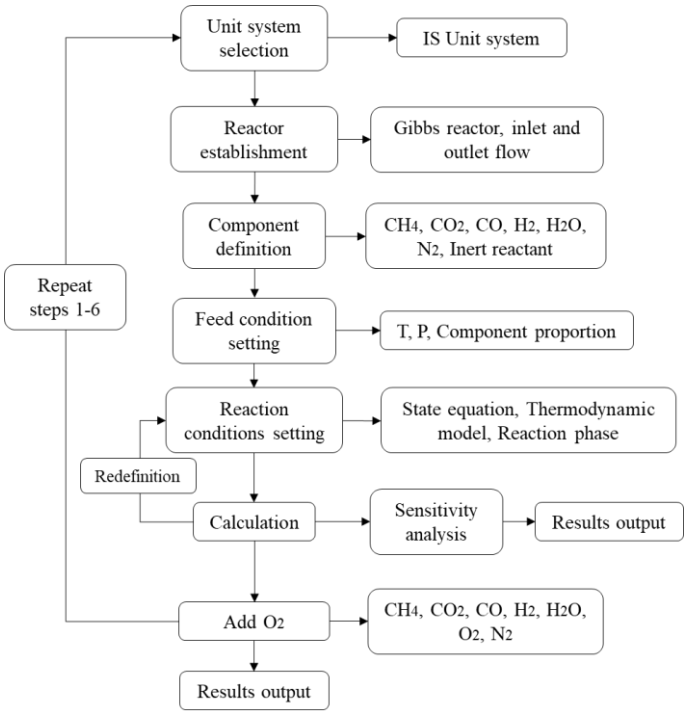


Figure S1 Flow chart of thermodynamic analysis

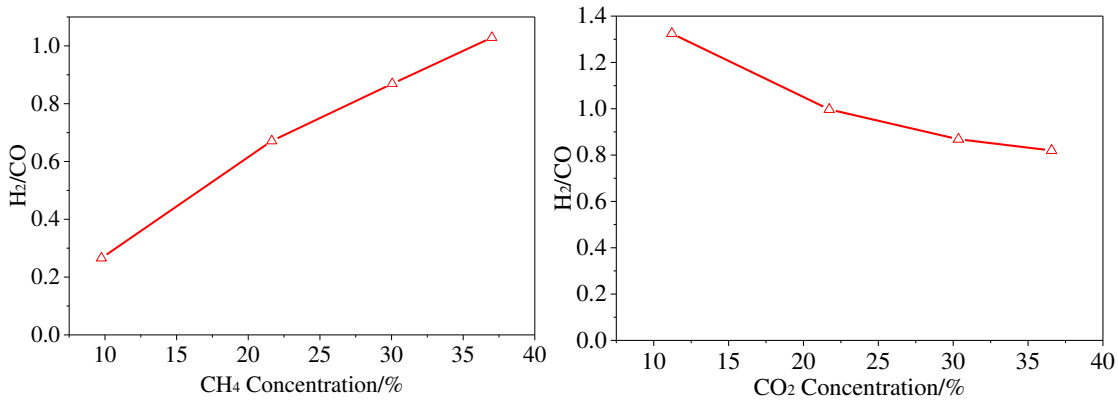


FigureS2 Effect of $CH_4$ and $CO_2$ on the ratio of $H_2/CO$（Catalyst dosage: 0.5 g; Reaction temperature: 800 °C; WHSV: 24000 $mL \cdot h^{-1} \cdot gcat^{-1}$）

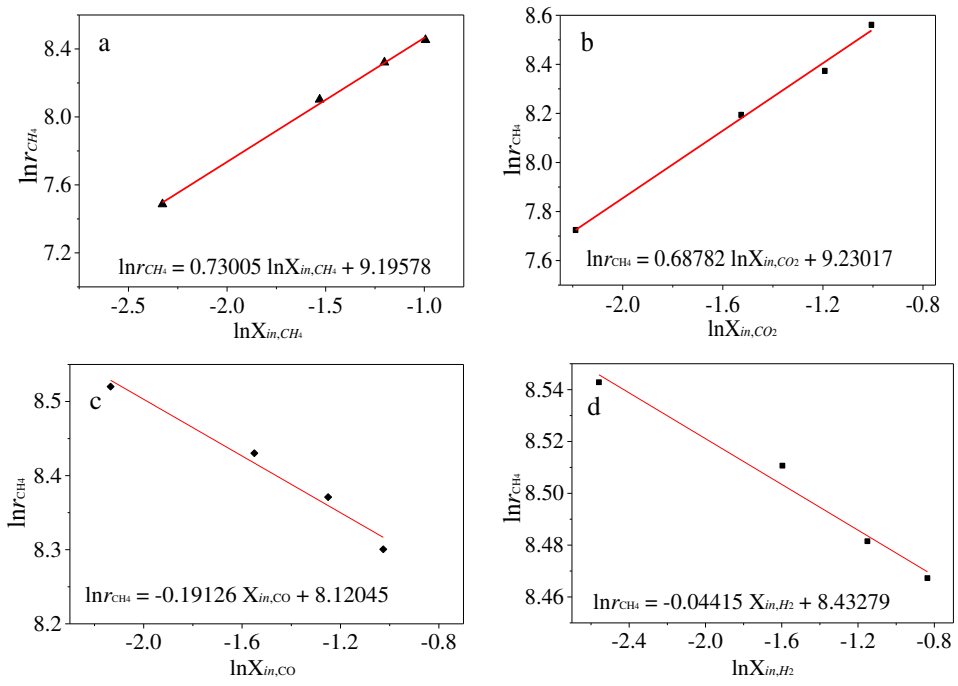


Figure S3 Calculation of different reaction orders (a: $CH_4$; b: $CO_2$; c: CO; d: $H_2$)

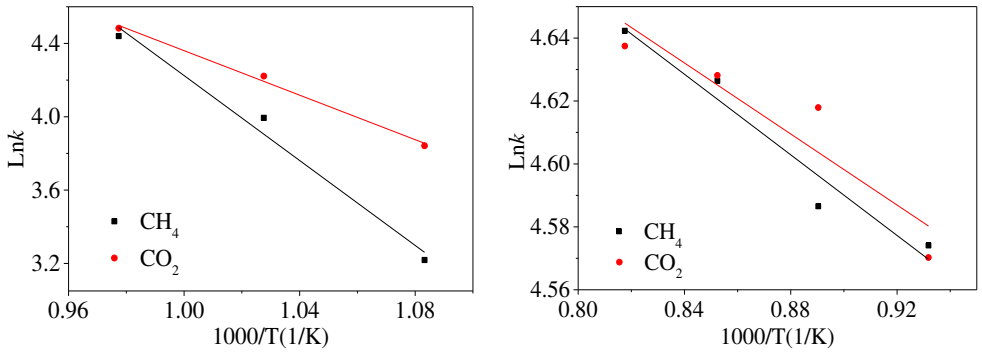


Figure S4 Calculation of different apparent activation energy (a: 650 ºC ~750 ºC; b: 800 ºC ~950 ºC)

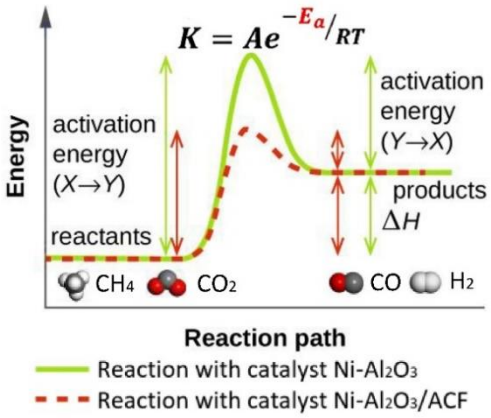


Figure S5 Schematic of reaction activation